BMB
Reports

BMB Rep. 2020; 53(3): 142-147
www.bmbreports.org

Sinapic acid induces the expression of thermogenic signature genes and lipolysis through activation of PKA/CREB signaling in brown adipocytes

Monir Hossain[1,2,#], Khan Mohammad Imran[1,2,#], Md. Shamim Rahman[1,2], Dahyeon Yoon[1,2], Vignesh Marimuthu[1,2] & Yong-Sik Kim[1,2,]*

[1]Institute of Tissue Regeneration, College of Medicine, Soonchunhyang University, Chenan 31151, [2]Department of Microbiology, College of Medicine, Soonchunhyang University, Cheonan 31151, Korea

Lipid accumulation in white adipose tissue is the key contributor to the obesity and orchestrates numerous metabolic health problems such as type 2 diabetes, hypertension, atherosclerosis, and cancer. Nonetheless, the prevention and treatment of obesity are still inadequate. Recently, scientists found that brown adipose tissue (BAT) in adult humans has functions that are diametrically opposite to those of white adipose tissue and that BAT holds promise for a new strategy to counteract obesity. In this study, we evaluated the potential of sinapic acid (SA) to promote the thermogenic program and lipolysis in BAT. SA treatment of brown adipocytes induced the expression of brown-adipocyte activation–related genes such as *Ucp1*, *Pgc-1α*, and *Prdm16*. Furthermore, structural analysis and western blot revealed that SA upregulates protein kinase A (PKA) phosphorylation with competitive inhibition by a pan-PKA inhibitor, H89. SA binds to the adenosine triphosphate (ATP) site on the PKA catalytic subunit where H89 binds specifically. PKA-cat-α1 gene–silencing experiments confirmed that SA activates the thermogenic program via a mechanism involving PKA and cyclic AMP response element–binding protein (CREB) signaling. Moreover, SA treatment promoted lipolysis via a PKA/p38-mediated pathway. Our findings may allow us to open a new avenue of strategies against obesity and need further investigation. [BMB Reports 2020; 53(3): 142-147]

*Corresponding author. Tel: +82-41-570-2413; Fax: +82-41-575-2412; E-mail: yongsikkim@sch.ac.kr
[#]These authors contributed equally to this work.

https://doi.org/10.5483/BMBRep.2020.53.3.093

Received 29 March 2019, Revised 3 May 2019, Accepted 14 June 2019

Keywords: Brown adipocyte, Browning, Lipolysis, PKA, Sinapic acid, UCP1

INTRODUCTION

Brown adipose tissue (BAT) in adult humans was discovered recently in imaging studies and has a function opposite to that of white adipose tissue (1). The unique feature of BAT is expression of UCP1, which helps to dissipate energy by diminishing the proton gradient in the inner membrane of mitochondria (2). Cold exposure of adult human obese and normal subjects has various physiologically beneficial effects such as increased glucose uptake and increased insulin sensitivity (3). In addition, cold exposure has been shown to cause BAT activation (4).

Thus, the well-known method for activation of BAT is cold exposure, which increases norepinephrine secretion and thermogenesis. In a study on a mouse model, it has been demonstrated that differentiation of brown fat is accompanied by mitochondrial biogenesis (5). Another study (on a brown preadipocyte cell line) has revealed that BMP7 treatment significantly increases the expression of genes involved in mitochondrial biogenesis and function, including *Pgc-1α* and *Nrf1* (6).

Certainly, PPARγ is the central regulator of both white fat and brown fat cell development. C/EBP family members function cooperatively with PPARγ and stimulate a transcriptional cascade to maintain a stable differentiated state of adipocytes. One report suggests that PPARγ is necessary for brown-fat development but not sufficient to drive the full brown-fat program (which requires additional factors) (7). Other studies offer evidence that transcriptional regulators including PPARγ, PGC-1α, PRDM16, and C/EBPβ can stimulate the development of brown fat (7, 8). Recently, research revealed that phytochemicals such as rutin activate brown fat, and cryptotanshinone promotes brown-adipocyte commitment among mesenchymal stem cells (9, 10).

In rodents, external stimuli lead to activation of β-adrenergic receptor 3 (β-3-AR) by sympathetic stimulation and increased cAMP production, which activates PKA and downstream genes of PKA (11). The activation of PKA promotes the release of fuel (free fatty acids) for thermogenesis. In mice, PKA modulates

ISSN: 1976-670X (electronic edition)

lipolysis activation involving β3-AR signaling which increases adenylyl cyclase activity and raises intercellular cAMP concentration (12). The elevated cAMP level triggers PKA, which phosphorylates HSL, ATGL, and perilipin, and thus subsequently initiates lipolysis (13). One report suggests that PKA upregulates UCP1 and plays role in both brown-adipocyte differentiation and mitochondrial biogenesis (11).

Sinapic acid (SA) is a natural alkaloidal amine found in black mustard seeds, wine, and vinegar. SA has been reported to have several biological functions, including antioxidant, anti-inflammatory, anticancer, antimicrobial, antimutagenic, and antianxiety activities (14). On the other hand, to date, the effects of SA on thermogenesis remain unexplored. In this study, we used BAT cells to find out the effect of SA on thermogenesis. We propose that SA holds promise as a potential secondary metabolite with a thermogenesis-promoting ability.

RESULTS

SA increases the expression of thermogenic markers and promotes mitochondrial biogenesis in brown adipocytes

During screening of 854 phytochemicals as described in our previous study (15) to find potential browning-thermogenic compounds, we found that SA can promote the activation of brown adipocytes. To decipher its function, at first, we tested the toxicity of SA toward brown adipocytes at indicated concentrations (Fig. 1A). It turned out that SA is not cytotoxic up to 72 h. Here, we compared the effects of SA with those of a well-known thermogenic inducer, Rosi, and BMP7 on the expression of thermogenic signature genes. SA treatment significantly enhanced *Ucp1* mRNA expression, by 1.8-fold (Fig. 1B). Additionally, SA treatment increased the mRNA expression levels of *Prdm16* (1.3-fold) and *Pgc-1α* (5.4-fold; Fig. 1B). As shown in Fig. 1C, SA treatment raised the protein expression levels of PRDM16, PGC-1α, PPARγ, and UCP1. The quantification data revealed that SA treatment increased UCP1 protein expression 1.7-fold, PGC-1α 1.9-fold, PRDM16 1.5-fold, and PPARγ protein expression 1.8-fold (Fig. 1C). It has been reported that PPARγ and PGC1α activation can promote mitochondrial biogenesis. So, we tested some of the mitochondrial-biogenesis-related genes: *Cox7a*, *Cox8b* and *Nrf1*. As shown in Fig. 2A, SA increased mitochondrial biogenesis related markers. Then, we performed immunostaining with MitoTracker and quantify the stain. As shown in Fig. 2B, SA treated cells showed higher mitochondrial mass than MDI. Next, we measured mtDNA expression and found that SA significantly increased mtDNA (Fig. 2C). After that, we needed to test whether mitochondrial biogenesis leads to increased

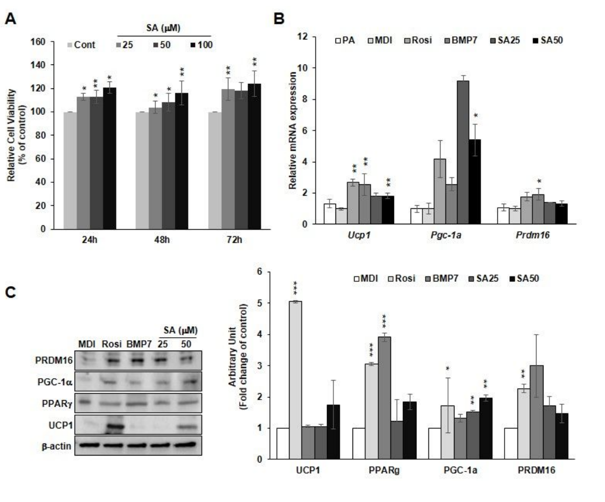

Fig. 1. SA induces expression of *Ucp1* along with other thermogenic genes. (A) Viability of brown adipocytes was assessed by the MTT assay at 24, 48, and 72 h. Data are expressed as mean ± SD of three independent experiments. qRT-PCR analysis was performed as described in the *Materials and Methods* section. (B) mRNA expression of brown-fat–specific markers: *Ucp1*, *Pgc-1α*, and *Prdm16*. Data are presented as mean ± SEM of three individual experiments. (C) Protein expression levels of brown-fat–specific markers UCP1, PRDM16, PPARγ, and PGC-1α. β-actin served as a loading control. Quantification of the protein expression levels of the brown-fat–specific markers. *A significant difference from group MDI (*P < 0.05, **P < 0.01, ***P < 0.001).

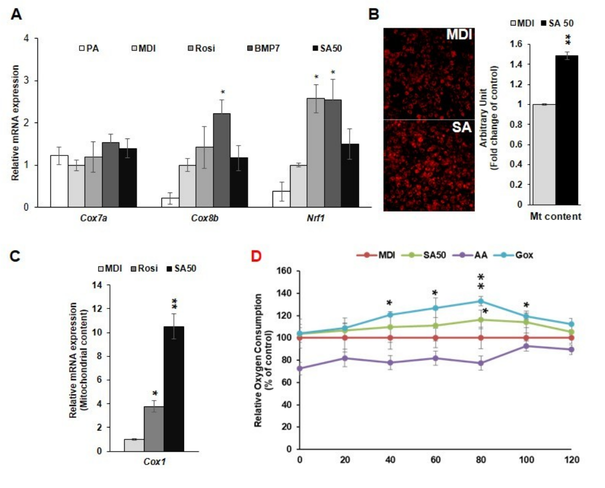

Fig. 2. SA increases mitochondrial biogenesis. (A) mRNA expression of mitochondrial-biogenesis-related markers: *Cox7a*, *Cox8b*, and *Nrf1*. Data are presented as mean ± SEM of three individual experiments. (B) MitoTracker immunostaining images of BAT cells. Data are representative of three independent experiments. Quantification of the immunostaining images. Data are expressed as mean ± SD of three independent experiments. (C) Relative mitochondrial *Cox1* DNA content (ratio of nDNA *p0* and mtDNA *Cox1*). (D) A Luxcel MitoXpress fluorescence assay was conducted to determine the oxygen consumption rate. Gox = glucose oxidase (positive control), AA = antimycin A (negative control). Data are shown as % of control (group MDI) ± SD from three independent experiments. *A significant difference from group MDI (*P < 0.05, **P < 0.01, ***P < 0.001).

oxygen consumption. As shown in Fig. 2D, SA treatment increased oxygen consumption. These data enabled us to propose that SA can induce the expression of thermogenic and mitochondrial biogenesis markers.

SA activates the PKA pathway in brown adipocytes

Of note, we found that SA and H89 share the ATP-binding pockets on the PKA surface via both hydrogen and hydrophobic interactions (Fig. 3A). SA and H89 seem to share amino acid residues Phe^{327}, Glu^{91}, Ala^{70}, Lys^{72}, Thr^{183}, Leu^{173}, Val^{57}, and Asp^{184} in the active site of PKA (Fig. 3A). Structural analysis revealed that the binding-affinity values of SA and H89 are −6.2 and −8.3 kcal/mol, respectively, implying that H89 binds more strongly than SA, but SA has the ability to slightly inhibit the activity of H89, as confirmed by western blotting (Fig. 3B). We increased the SA concentration and treated PKA with H89; we found that SA treatment inhibited the H89 activity (Fig. 3B). The molecular docking analysis suggests that SA may be a potent agonist for induction of PKA phosphorylation.

On the basis of this finding, we investigated PKA signaling during SA treatment. We found that SA treatment increases PKA substrate phosphorylation at 60 min as compared to the MDI medium (Fig. 3C). We also tested the phosphorylation of other downstream kinases of PKA signaling, where we found that SA stimulates phosphorylation of CREB, p38, and ERK as well (Fig. 3D). We also observed that SA treatment promoted phosphorylation of HSL (Ser^{563} and Ser^{660}) on day 6 during brown-adipocyte differentiation (Fig. 3E). In addition, we assessed triglyceride (TG) accumulation by ORO staining (Supplemental Fig. 1A and B).

To understand the function of SA in thermogenic gene induction, we confirmed the expression of PKA downstream genes, *Ucp1*, *Pgc1α* and *Prdm16* in SA treated condition along with an activator of cAMP-dependent protein kinase, 8-bromoadenosine 3′.5′-cyclicmomophosphate (8-Br-cAMP) (Fig. 4A and 4B). Data suggested SA can effectively induce thermogenic genes. To confirm PKA signaling in SA-treated brown adipocytes, we tried to assess the effect of PKA inhibition on SA-mediated PKA substrate phosphorylation (Fig. 4C and 4D). The expression of downstream thermogenic target genes of PKA, e.g., *Ucp1*, *Pgc1α*, *Pparγ*, and *Cebpα* was diminished by H89 treatment, but this effect was reversed by cotreatment with SA (Fig. 4C). As depicted in Fig. 4D, HSL (Ser^{563} and Ser^{660}) and CREB (Ser^{133}) phosphorylation was dramatically inhibited during H89 treatment. By contrast, during cotreatment with SA, the phosphorylation was significantly recovered.

We next studied the activities of the PKA signaling pathway during *PKA-cat-α1* gene silencing and SA treatment (Fig. 4E). As illustrated in Fig. 4E, PKA-cat-αl siRNA inhibited the mRNA expression of *PKA-cat-αl* effectively. As expected, the expression of the downstream genes in the PKA signaling pathway was reduced by *PKA-cat-αl* gene silencing, but this

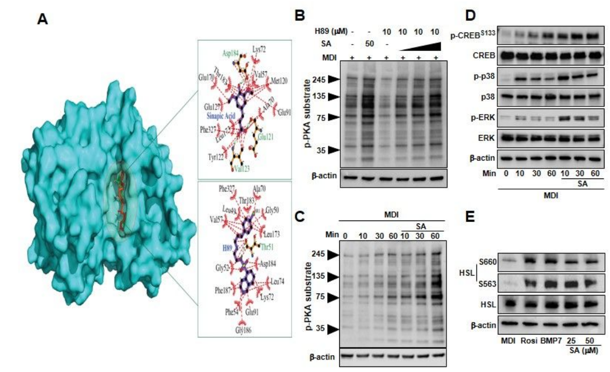

Fig. 3. SA activates PKA pathways in BAT cells. (A) Structural analysis of SA and the pan-PKA inhibitor H89 in complex with PKA. They share the same binding pocket on the PKA surface, and the active-site amino acid residues Phe^{327}, Glu^{91}, Ala^{70}, Lys^{72}, Thr^{183}, Leu^{173}, Val^{57}, and Asp^{184} were found to be common for the interactions of SA and H89 with PKA. (B) Competition between the pan-PKA inhibitor H89 and SA. (C) WB images of phosphorylation levels of PKA substrates during SA (50 μM) treatment at the indicated time points. (D) Phosphorylation of CREB (Ser^{133}), p38, and ERK during SA (50 μM) treatment at the indicated time points. (E) WB images of phosphorylation levels of HSL (Ser^{563} and Ser^{660}) under the influence of SA treatment. Rosi: Rosiglitazone, BMP7: bone morphogenic protein 7. β-actin was used as a loading control.

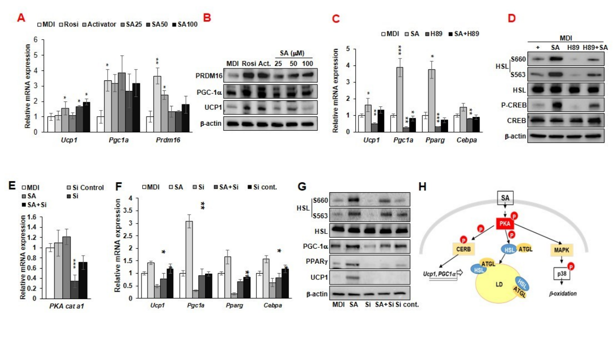

Fig. 4. The function of PKA in SA-mediated differentiation of brown adipocytes. (A, B) Comparison of PKA downstream targets after SA and PKA activator, 8-bromoadenosine 3′.5′-cyclicmomophosphate (8-Br-cAMP) treatment. (C, D) The expression of PKA downstream targets after SA (50 μM) and/or H89 (10 μM) treatment. (E, F) mRNA expression levels of *PKA-cat-α1* and downstream target genes of PKA, e.g., *Ucp1*, *Pgc-1α*, *Pparγ*, and *Cebpα* in BAT cells (6 days of differentiation) after the knockdown of the *PKA-cat-α1* gene. Data are expressed as mean ± SEM of three independent experiments. *A significant difference from group MDI (*P < 0.05, **P < 0.01, ***P < 0.001). (G) Protein expression of PKA's downstream genes (*Ucp1*, *Pparγ*, *Pgc-1α*, and *Hsl*) and phosphorylation levels of HSL (Ser^{563} and Ser^{660}) in BAT cells (6 days of differentiation) after the knockdown of the *PKA-cat-α1* gene. (H) A schematic model of SA-mediated lipolysis and differentiation of brown adipocytes via the PKA pathway.

effect was attenuated by SA treatment (Fig. 4F and 4G). Overall, we can propose that SA contributes to brown-adipocyte activation and lipolysis via activation of PKA signaling (Fig. 4H).

DISCUSSION

Stimulation of brown adipocytes and UCP1 mediated heat production require activation of adipocytes and muscle cell surface receptors, such as Trpv1, β3-AR, Ptch1, A2aR and TrkB. These receptors require cellular signaling cascades such as PKA, PKG, Sirt1, AMPK, and p38 MAPK, cytokines (IL-4 and IL-13), and transcriptional regulators, such as Prdm family, Pgc-1α, Ppar family, and Zfp516 for UCP1 expression (16).

Several plant-extracted compounds (berberine, butein, capsaicin, and fucoxanthin), artificially synthesized compounds (e.g., a Pparγ agonist, β3-AR agonist, and salsalate), and endogenous small-molecule factors (e.g., serotonin, lactate, and adenosine) have been identified as potential BAT activators that turn on thermogenic transcriptional factors by involving their cell surface receptors or by cellular signaling cascades modulation (16). Our data revealed that SA acts as a potent stimulator of brown-adipocyte activation. The protein factors that control brown-fat differentiation were upregulated by SA treatment, including PPARγ, PGC-1α, CEBPβ, and PRDM16 along with increased expression of UCP1. mRNA and protein expression levels of a key thermogenic marker, UCP1, were increased by SA treatment here, indicating activation of mature BAT adipocytes. HSL activity appears to be regulated by site-specific phosphorylation on at least five serine residues (Ser^{563}, Ser^{565}, Ser^{600}, Ser^{659}, and Ser^{660}), and PKA phosphorylates HSL at Ser^{563}, Ser^{659}, and Ser^{660} (17, 18). SA increases the phosphorylation of HSL (Ser^{563} and Ser^{660}); during browning and during thermogenic activation of BAT, similar changes with increased lipolysis have been observed (19).

The differentiation and physiological functions of brown adipocytes are closely related to enhance mitochondrial biogenesis. Researcher has demonstrated that PPARγ and transcriptional coactivator PGC-1α can contribute to mitochondrial function and biogenesis (20) which are similar to our findings although further investigation is needed for molecular mechanism.

Computational identification of PKA agonist has been described elsewhere (21) where, lead compound share same binding site as SA, but described as an agonist of PKA. H89 inhibits the activation of CREB and the CREB-mediated MKP-1 induction by lipopolysaccharide (LPS) resulting from the inhibition of PKA and MSK by H89 (22). Protein kinases catalyzes the transfer of γ-phosphate of ATP to the hydroxyl group present in a tyrosine, serine, or threonine residue to phosphorylate their substrates. The direct effects of H89 on active site of the enzyme causes its inhibitory actions. It also looked likely that H89 obstructs protein kinase activity via interacting with the free enzyme, not with the enzyme–ATP complex (23). PKA mediates forskolin-induced CREB phosphorylation through p38 and MSK1 in NIH 3T3 cells (24). In our study, H89 treatment inhibited PKA phosphorylation resulting lower effect of SA on HSL phosphorylation at PKA target sites, Ser^{563} and Ser^{660}; our data are in agreement with the findings of other researchers (25). SA and H89 both can bind competitively to PKA by sharing the ATP-binding site on a PKA catalytic subunit, as we showed by our molecular docking analysis and confirmed by western blotting. Our data indicate that the expression of target genes of PKA, e.g., *Ucp1*, *Pgc1α*, *Pparγ*, and *Cebpβ*, was reduced by H89 treatment, but this suppression was reversed by SA treatment. Besides, SA promoted phosphorylation of CREB, p38, and ERK; CREB phosphorylation was inhibited by H89 treatment, and this change was attenuated by SA treatment. In this context, we propose that SA-mediated PKA activation can induce both phosphorylation of its downstream targets and expression of browning-related genes although a fine-tuned study is needed to confirm this crosstalk.

In conclusion, this study revealed that SA not only activates the thermogenic program but also induces lipolysis. SA-mediated thermogenic-signature upregulation is probably involved in the activation of UCP1 via PKA/CREB signaling. Our findings may open up a new avenue of research on the downstream thermogenic program in *in vivo* models.

MATERIALS AND METHODS

Chemicals, reagents, and antibodies

SA (purity ≥ 98.0%), insulin, dexamethasone, 3-isobutyl-1-methylxanthine (IBMX), rosiglitazone (Rosi), 8-bromoadenosine 3′.5′-cyclicmomophosphate (8-Br-cAMP), Oil Red O dye (ORO), and 3-(4,5-dimethylthiazol-2-yl)-2,5-diphenyltetrazolium bromide (MTT) were purchased from Sigma-Aldrich (St. Louis, MO, USA), and human recombinant BMP7 from R & D Systems (Minneapolis, MN, USA). Fetal bovine serum (FBS) and High-glucose Dulbecco's modified Eagle's medium (DMEM) were bought from Atlas Biologicals (Fort Collins, CO, USA), and a penicillin-streptomycin solution from Hyclone Laboratories, Inc. (South Logan, NY, USA). Antibodies against UCP1, PGC-1α, PRDM16, and β-actin were purchased from Abcam (Cambridge, MA, USA), whereas antibodies against phospho-HSL (Ser^{563} and Ser^{660}) and HSL from Cell Signaling Technology (Danvers, MA, USA).

Cell maintenance and differentiation

BAT cells were cultured and maintained in the DMEM GlutaMax medium supplemented with 10% of FBS and 1% of the penicillin-streptomycin solution and were kept at 37°C in a 5% CO_2 incubator. BAT cells are an immortalized cell line created by Lee BS group (26). The cells were differentiated as described elsewhere (27). Cells after 6 days of differentiation were used in all the experiments unless stated otherwise.

Cell treatment procedures

Fully confluent BAT cells were treated with the MDI differentiation induction medium consisting of 0.5 mM 3-isobutyl-1-methylxanthine, 1 μM dexamethasone, and 10 μg/ml insulin in DMEM supplemented with 10% of FBS, followed by a maturation medium composed of DMEM, 10% of FBS, and 10 μg/ml insulin. The media were refreshed every other day. The following treatment groups were set up: MDI, Rosi with MDI (positive control), BMP7 with MDI (positive control), and SA with MDI. Treatments exceeding 2 days were continued until day 4 by mixing drugs with the maturation medium. After day 4, only the maturation medium was used until cell harvesting. Preadipocytes were maintained only in the culture medium (DMEM and 10% of FBS).

Cell viability assay

In 96-well plates, BAT cells were seeded at 80% to 90% confluence. Cell viability was evaluated by MTT assay as described elsewhere (15).

Analysis of mitochondrial DNA content

Mitochondrial biogenesis was quantified by real-time qPCR as described elsewhere (28) assuming that the ratio of mitochondrial DNA (mtDNA) to nuclear DNA (nDNA) increases but nDNA remains constant.

Oxygen consumption assay

BAT cells were seeded in a 96-well plate at a density of approximately 40,000-60,000 cells per well. Oxygen consumption assay was performed as kit protocol (Cayman, Ann Arbor, MI, USA).

Quantitative reverse-transcription PCR (qRT-PCR) analyses

Total-RNA extraction from (and qRT-PCR analyses of) BAT cells were performed as described previously (29). The primer sequences employed in this study are listed in Supplemental Table 1. Expression of target genes was normalized to that of TATA box–binding protein (*Tbp*).

Preparation of whole-cell extracts for western blot (WB) analyses

Whole-cell extracts from BAT cells were prepared as described elsewhere (30) with a minor modification. Briefly, cell extracts were collected after 6 days of differentiation. Next, 1% BSA was used for blocking the membranes instead of skim milk (because of analysis of phosphoproteins), and a phosphatase inhibitor cocktail (Sigma-Aldrich) was added into RIPA lysis buffer (Santa Cruz Biotechnology, Inc.).

Gene silencing experiments

Gene silencing assay was conducted as described previously (31).

In silico analysis

Western blot analysis revealed that SA upregulates phosphorylation of PKA in the absence of inhibitor H89 and attenuates H89-mediated dephosphorylation. To understand the mechanism better, molecular-docking–based structural analysis was performed. First, crystal structure of cAMP-dependent protein kinase (PDB ID: 1BX6) with a potent inhibitor, balanol (a natural product), bound to its catalytic subunit was obtained from Protein Data Bank (www.rcsb.org). After that, the ligand was removed, and a binding grid of (40 × 40 × 40, 1 Å) size was generated containing all possible active sites on PKA surface. Before docking, all the structures were prepared with AutoDock Tools (32), polar hydrogen was added, and finally molecular docking was performed in the AutoDock Vina software (33).

Statistics

Data are representative of three or more experiments and are shown as mean ± standard error of the mean (SEM). Student's *t* test was conducted to identify significant changes between a control group and various treatment groups. Data with a P value of < 0.05 were considered statistically significant.

ACKNOWLEDGEMENTS

This research was supported by the Basic Science Research Program through the National Research Foundation of Korea (NRF) funded by the Ministry of Education (2015R1A6A1030 32522), and partially by a research fund of Soonchunhyang University.

CONFLICTS OF INTEREST

The authors have no conflicting interests.

REFERENCES

1. Vijgen GH, Sparks LM, Bouvy ND et al (2013) Increased oxygen consumption in human adipose tissue from the "brown adipose tissue" region. J Clin Endocrinol Metab 98, E1230-E1234
2. Nedergaard J, Golozoubova V, Matthias A, Asadi A, Jacobsson A and Cannon B (2001) UCP1: the only protein able to mediate adaptive non-shivering thermogenesis and metabolic inefficiency. Biochim Biophys Acta Bioenerg 1504, 82-106
3. Chondronikola M, Volpi E, Børsheim E et al (2014) Brown adipose tissue improves whole-body glucose homeostasis and insulin sensitivity in humans. Diabetes 63, 4089-4099
4. Saito M, Yoneshiro T and Matsushita M (2016) Activation and recruitment of brown adipose tissue by cold exposure and food ingredients in humans. Best Pract Res Clin Endocrinol Metab 30, 537-547
5. Uldry M, Yang W, St-Pierre J, Lin J, Seale P and Spiegelman BM (2006) Complementary action of the PGC-1 coactivators in mitochondrial biogenesis and

brown fat differentiation. Cell Metab 3, 333-341
6. Xue R, Wan Y, Zhang S, Zhang Q, Ye H and Li Y (2013) Role of bone morphogenetic protein 4 in the differentiation of brown fat-like adipocytes. Am J Physiol Endocrinol Metab 306, E363-E372
7. Kajimura S, Seale P and Spiegelman BM (2010) Transcriptional control of brown fat development. Cell Metab 11, 257-262
8. Seale P, Kajimura S, Yang W et al (2007) Transcriptional control of brown fat determination by PRDM16. Cell Metab 6, 38-54
9. Yuan X, Wei G, You Y et al (2016) Rutin ameliorates obesity through brown fat activation. FASEB J 31, 333-345
10. Imran KM, Rahman N, Yoon D, Jeon M, Lee BT and Kim YS (2017) Cryptotanshinone promotes commitment to the brown adipocyte lineage and mitochondrial biogenesis in C3H10T1/2 mesenchymal stem cells via AMPK and p38-MAPK signaling. Biochim Biophys Acta Mol Cell Biol Lipids 1862, 1110-1120
11. Sell H, Deshaies Y and Richard D (2004) The brown adipocyte: update on its metabolic role. Int J Biochem Cell Biol 36, 2098-2104
12. Duncan RE, Ahmadian M, Jaworski K, Sarkadi-Nagy E and Sul HS (2007) Regulation of lipolysis in adipocytes. Annu Rev Nutr 27, 79-101
13. Zimmermann R, Lass A, Haemmerle G and Zechner R (2009) Fate of fat: the role of adipose triglyceride lipase in lipolysis. Biochim Biophys Acta Mol Cell Biol Lipids 1791, 494-500
14. Nićiforović N and Abramovič H (2014) Sinapic acid and its derivatives: natural sources and bioactivity. Compr Rev Food Sci Food Saf 13, 34-51
15. Imran KM, Yoon D, Lee TJ and Kim YS (2018) Medicarpin induces lipolysis via activation of Protein Kinase A in brown adipocytes. BMB Rep 51, 249-254
16. Song NJ, Chang SH, Li DY, Villanueva CJ and Park KW (2017) Induction of thermogenic adipocytes: molecular targets and thermogenic small molecules. Exp Mol Med 49, e353
17. Watt MJ, Holmes AG, Pinnamaneni SK et al (2006) Regulation of HSL serine phosphorylation in skeletal muscle and adipose tissue. Am J Physiol Endocrinol Metab 290, E500-E508
18. Anthonsen MW, Rönnstrand L, Wernstedt C, Degerman E and Holm C (1998) Identification of novel phosphorylation sites in hormone-sensitive lipase that are phosphorylated in response to isoproterenol and govern activation properties in vitro. J Biol Chem 273, 215-221
19. Barneda D, Frontini A, Cinti S and Christian M (2013) Dynamic changes in lipid droplet-associated proteins in the "browning" of white adipose tissues. Biochim Biophys Acta Mol Cell Biol Lipids 1831, 924-933
20. Corona JC and Duchen MR (2015) PPARγ and PGC-1α as therapeutic targets in Parkinson's. Neurochem Res 40, 308-316
21. Natarajan P, Swargam S, Hema K, Vengamma B and Umamaheswari A (2015) E-pharmacophore based virtual screening to identify agonist for PKA-Cα. Biochem Anal Biochem 4, doi:10.4172/2161-1009.1000222
22. Cho IJ, Woo NR, Shin IC and Kim SG (2009) H89, an inhibitor of PKA and MSK, inhibits cyclic-AMP response element binding protein-mediated MAPK phosphatase-1 induction by lipopolysaccharide. Inflamm Res 58, 863-872
23. Lochner A and Moolman J (2006) The many faces of H89: a review. Cardiovasc Drug Rev 24, 261-274
24. Delghandi MP, Johannessen M and Moens U (2005) The cAMP signalling pathway activates CREB through PKA, p38 and MSK1 in NIH 3T3 cells. Cell Signal 17, 1343-1351
25. Watt MJ and Cheng Y (2017) Triglyceride metabolism in exercising muscle. Biochim Biophys Acta Mol Cell Biol Lipids 1862, 1250-1259
26. Park JH, Kang HJ, Kang SI et al (2013) A multifunctional protein, EWS, is essential for early brown fat lineage determination. Dev Cell 26, 393-404
27. Rosenwald M, Perdikari A, Weber E and Wolfrum C (2013) Phenotypic analysis of BAT versus WAT differentiation. Curr Protoc Mouse Biol 3, 205-216
28. Schild L, Dombrowski F, Lendeckel U, Schulz C, Gardemann A and Keilhoff G (2008) Impairment of endothelial nitric oxide synthase causes abnormal fat and glycogen deposition in liver. Biochim Biophys Acta Mol Basis Dis 1782, 180-187
29. Rahman N, Jeon M and Kim YS (2016) Delphinidin, a major anthocyanin, inhibits 3T3-L1 pre-adipocyte differentiation through activation of Wnt/β-catenin signaling. Biofactors 42, 49-59
30. Jeon M, Rahman N and Kim YS (2016) Wnt/β-catenin signaling plays a distinct role in methyl gallate–mediated inhibition of adipogenesis. Biochem Biophys Res Commun 479, 22-27
31. Yoon D, Imran KM and Kim YS (2018) Distinctive effects of licarin A on lipolysis mediated by PKA and on formation of brown adipocytes from C3H10T1/2 mesenchymal stem cells. Toxicol Appl Pharmacol 340, 9-20
32. Morris GM, Huey R, Lindstrom W et al (2009) AutoDock4 and AutoDockTools4: Automated docking with selective receptor flexibility. J Comput Chem 30, 2785-2791
33. Trott O and Olson AJ (2010) AutoDock Vina: improving the speed and accuracy of docking with a new scoring function, efficient optimization, and multithreading. J Comput Chem 31, 455-461